Expansion and degradation of cement paste in sodium sulfate solutions

Ma, Xu; Copuroglu, Oguzhan; Schlangen, Erik; Han, Ningxu; Xing, Feng

DOI
10.1016/j.conbuildmat.2017.10.026

Publication date
2018

Document Version
Final published version

Published in
Construction and Building Materials

Citation (APA)
Ma, X., Copuroglu, O., Schlangen, E., Han, N., & Xing, F. (2018). Expansion and degradation of cement paste in sodium sulfate solutions. *Construction and Building Materials*, *158*, 410-422. https://doi.org/10.1016/j.conbuildmat.2017.10.026

Construction and Building Materials 158 (2018) 410–422

Contents lists available at ScienceDirect

Construction and Building Materials

journal homepage: www.elsevier.com/locate/conbuildmat

Expansion and degradation of cement paste in sodium sulfate solutions

Xu Ma [a,b,*], Oğuzhan Çopuroğlu [a], Erik Schlangen [a], Ningxu Han [b], Feng Xing [b]

[a] Delft University of Technology, Stevinweg 1, 2628 CN Delft, The Netherlands
[b] Guangdong Province Key Laboratory of Durability for Marine Civil Engineering, Shenzhen University, Shenzhen 518060, PR China

HIGHLIGHTS

- The expansion behavior was investigated based on strain gauge measurement system.
- The change of sulfur distribution was studied by EDS elemental mapping.
- The crack development was discussed based on BSE micrograph and CT scanning.
- The experimental results offered the needed information for further numerical study.

ARTICLE INFO

Article history:
Received 27 July 2017
Received in revised form 1 October 2017
Accepted 3 October 2017
Available online 15 October 2017

Keywords:
External sulfate attack
Expansion
Stress
Pore size distribution
Sulfur distribution
Crack pattern

ABSTRACT

External sulfate attack is a progressive degradation process that may cause expansion, cracking, loss of binder cohesion and increased permeability in cementitious materials. Crystallization pressure theory has often been referred to as the most likely mechanism. However, thus far the stress causing the expansion has not been quantified. In this study, small cement paste pipes with a wall thickness of 2.5 mm were prepared and immersed in sodium sulfate solutions with SO_4^{2-} ion concentrations of 1.5 g/L and 30 g/L. Three types of longitudinal restraints were applied on the specimens before exposure, which were created by a spring, a thin or a thicker stainless steel bar that was centered in the hollow specimens in order to facilitate the non-, low- or high-restraint condition. The free expansion, restrained expansion and generated stress were quantified. The pore size distribution, sulfur distribution and crack pattern were periodically analyzed during the sulfate immersion tests up to 420 days. The generated stresses were found to be as high as 13.1 MPa in high sulfate solution and 8.3 MPa in low sulfate solution under high-restraint condition after 420-day immersion. For the unrestrained specimens immersed in low sulfate solution, an almost uniform sulfur distribution along the diffusion direction was found at 189-day immersion. However, for the unrestrained specimens immersed in high sulfate solution, a layer or several layers of mainly gypsum were formed subparallel to the exposed surface from 133-day immersion.

1. Introduction

External sulfate attack is a progressive degradation of cementitious materials upon being exposed to external sulfate ions. It is a complex issue in which ionic transport, expansive reactions and mechanical damage are responsible in varying degrees for gradually increased macroscopic expansion and severe mechanical damage [1–3]. Sulfate ions present in seawater, rivers, groundwater and industrial effluent can penetrate into the hardened concrete, and react with cement hydration products to form ettringite as well as gypsum crystals, if higher sulfate concentrations are available [4–7]. Such formations result in a solid volume increase and cause local expansive stress within the pore network. Although the solid volume increase may initially reduce the porosity of cement paste, it will cause cracking at a later stage as the generated expansive stress exceeds the tensile strength of cement paste. This, in turn, leads eventually to a total strength loss and an increased permeability of concrete.

Even though the theories concerning the exact origin of the expansive stresses are under debate, ettringite formation from monosulfate is generally considered as the major cause [8–11]. Lothenbach et al. [10] showed that the increase in solid volume caused by external sulfate attack did not exceed the total capillary porosity and concluded that the formation of ettringite within the matrix leads to the observed expansion. Yu et al. [9] provided evidence that sulfate related expansion is linked to the formation of ettringite from monosulfate crystals embedded within the C-S-H. Müllauer et al. [8] concluded that the damage is due to the

* Corresponding author at: Delft University of Technology, Stevinweg 1, 2628 CN Delft, The Netherlands.
E-mail address: X.Ma-1@tudelft.nl (X. Ma).

https://doi.org/10.1016/j.conbuildmat.2017.10.026
0950-0618/

formation of ettringite in small pores (10–50 nm) which generates stresses up to 8 MPa exceeding the tensile strength of the binder matrix. Ettringite formation also takes place in larger pores, but the generated stress is negligible. In this case, the most likely expansion mechanism can be the crystallization pressure developing inside the nanopores within the cement paste.

According to the crystallization pressure theory [12–15], the driving force for crystallization pressure is the supersaturation of the pore solution. Then, the crystal growth in the confined space leads to the expansive stress on the pore walls. An inverse relationship between the expansive stress and the pore size is critical. Müllauer et al. [8] calculated a spherical crystal with a radius of around 25 nm and found that this is in equilibrium at a maximum stress of around 8 MPa. Yu et al. [9] also calculated the crystallization pressure as high as 21 MPa from a supersaturated solution to form ettringite. The magnitude of the expansive stress on the walls of nanopores can be predicted based on the crystallization pressure theory. However, an experimental verification is still missing since direct measurement of the expansive stress on nanopore walls is highly challenging. Therefore, the authors propose determining the expansive stress indirectly through modeling the expansion behavior of larger scale specimens under various degrees of restraint, which can be verified by the experiments.

External sulfate attack under continuous immersion condition is a slow diffusion process. Even though high water/cement ratios and high sulfate ion concentrations have been adopted as acceleration methods, research shows that the attack depth remains shallow even after several months [9,16]. Therefore, specimens with a small thickness along the diffusion direction could be preferred for experimental research in order to ensure a faster exposure of the entire cross-section. Müllauer et al. [8] considered the problem mentioned above in their research. The thin-walled hollow mortar cylinders with a wall thickness of 2.5 mm and the specially constructed stress cell with different diameters of central steel bars were used as their experimental setup. The expansion behavior and generated stress of mortar pipe were studied. In our research, in order to eliminate the influence of aggregates and reach a relatively uniform distribution of local expansion stress at each attack depth, cement paste specimens were chosen over mortar and concrete. Strain gauges were used for the measurements of restrained expansions and generated stresses, with the purposes of increasing the measurement accuracy and obtaining continuous experimental results. Sulfur distributions at different immersion time and crack developments caused by external sulfate attack were also studied.

The ingress of the external sulfate ions is a process, which involves a dynamic local expansive stress gradient along the diffusion direction. Therefore, the sulfur profile and the pore size distribution within the same depth were determined in this research. Theoretically, the dynamic local expansive stress gradient is related with the dynamic sulfur gradient, which can offer the needed information for the input of the modeling. The reader is referred to Ma et al. [17] for the framework of modeling of this mechanism. The outputs of the model are expansion, generated stress and crack pattern, which can be validated by the experimental results. Therefore, all the experimental results presented in this paper were expected to contribute significantly to the simulations including a gradient distribution of local expansive stress along the diffusion direction, which reflects the process of external sulfate attack. This research aims at understanding the relationship between the local expansive stresses generated within nanopores and the global expansion characteristics through computational simulations and experimental methods. This paper focuses on the experimental results.

2. Experimental approach

2.1. Specimen preparation and test setup

An ordinary Portland cement (CEM I 42,5 N) with a water/cement ratio of 0.40 was used in this study. PVC moulds with stainless steel rods in the center (Fig. 1) were fabricated in order to produce the cement paste pipes with a wall thickness of 2.5 mm (outer diameter 30 mm, inner diameter 25 mm), based on the earlier study of Müllauer et al. [8,18]. During casting of the cement paste pipes, the moulds were put on a vibration table to make the casting easier and also remove the air from the fresh paste. Then the unmoulded specimens were wrapped with plastic foil and kept in curing room (20 ± 1 °C, 96 ± 2 % RH) for 24 h. After that, the specimens were demoulded and cured in saturated lime-water at 20 ± 1 °C for another 90 days [17]. Upon completion of the curing period, the cement paste pipes were cut and polished at both ends to ensure that they were parallel and that the length was 70 mm.

Three types of longitudinal restraints were applied on the cement paste pipes in this study [8,17]. The restraints were created by a spring, a thin stainless steel bar or a thicker stainless steel bar that were centered in the pipes in order to facilitate the non-, low- or high-restraint condition (Fig. 2). The middle part diameters of thin steel bars and thick steel bars are 3 mm and 7 mm, respectively. Strain gauges were used for the thin and thick steel bars to measure the deformation of the bars and determine the restraint and resulting stresses. In order to reduce the influence of bending during tests, two strain gauges were glued on the opposite side of the middle part of each steel bar, and the average reading of the two strain gauges was used as the final strain. Then a special coating was applied on the surfaces of strain gauges to protect the strain gauges when exposed to sulfate solutions. The strain values of the strain gauges were measured continuously with a CompactDAQ system connected to a computer.

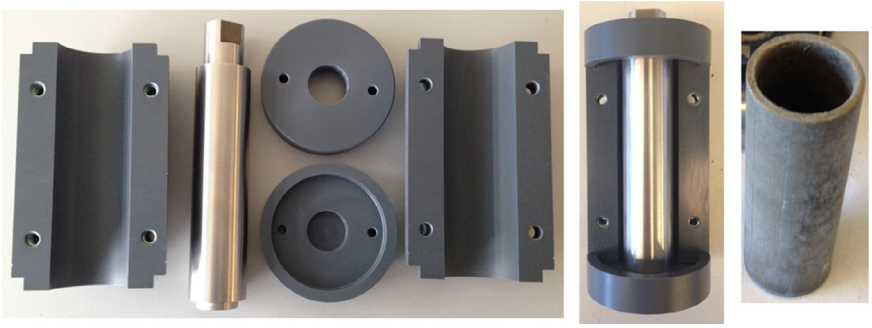

Fig. 1. PVC moulds and specimens.

Fig. 2. Three types of restraints; A) thick steel bar, B) thin steel bar and C) spring.

After 90 days of curing in saturated limewater, the cement paste pipes were assembled with the three types of longitudinal restraints. In order to ensure a firm contact between the steel disks and specimens under low- and high-restraint conditions, 0.7 N m was imposed on the nuts with a precision torque wrench. Then the whole system was immersed in sodium sulfate solutions with the SO_4^{2-} ion concentrations of 1.5 g/L and 30 g/L, attempting to account for natural and accelerating conditions, respectively. For each exposure condition, five additional specimens were immersed in sulfate solutions, however these additional specimens did not have any restraint thus were able to expand freely. These free expanding specimens were used for MIP (mercury intrusion porosimetry), SEM (scanning electron microscope) – EDS (energy dispersive X-ray spectrometry) microanalysis and CT (X-ray computed tomography) scanning. The immersion tests were carried out in a room with a constant temperature at 20 ± 1 °C. The temperature of each sulfate solution was monitored by temperature sensors during the tests, considering the sensitivity to temperature change of steel bars and strain gauges. The sulfate solutions were renewed every two weeks until 238-day immersion and from there on every four weeks to keep the strength of the solution stable.

2.2. Calculations of expansion and generated stress

In this paper, expansion is expressed as the strain of the cement paste pipe along the longitudinal direction, which is equal to the increased length divided by the original length of the cement paste pipe (70 mm). The free expansion stands for the expansion under non-restraint condition with a spring being assembled, which was measured at every 14 days up to a total of 98-day immersion. After that, the measurements were carried out at every 7 days. For every measurement, the specimens were taken out from the solutions and the length differences were recorded by comparing with a reference steel rod using a digital indicator. The measurement process was finished very fast to prevent the specimens from drying. The reference steel rod was kept in a constant temperature room to avoid temperature influences.

The restrained expansion represents the expansion under low- or high-restraint condition created by a thin steel bar (3 mm) or a thicker steel bar (7 mm). The generated stress means the compressive stress acting on the cement paste pipe at the restrained boundaries due to the restraint by the steel bars, which was originally caused by the interaction between the external sulfate ions and the hydration products. The specimens were expected to expand because of external sulfate attack. Therefore, the steel bars were under tensile force, which lead to the same compressive force on the specimens. During the immersion tests, the readings of the strain gauges were recorded continuously. Then the restrained expansions and the generated stresses were calculated based on the obtained strain values of the strain gauges. However, two types of calibrations of the strain gauge measurement system were needed for the calculations, which were done before the immersion tests. The two types of calibrations were the tensile test calibration and the torque test calibration, with the purposes of obtaining the stress–strain curves and the relationship between local strain and total strain of the steel bars, respectively.

During the tensile test of each steel bar, the strain of the strain gauges and the applied tensile force were recorded. Then the stress–strain curve of each steel bar was acquired, where the strain in the curve is from the strain gauges. During the immersion tests, the readings of the strain gauges were recorded continuously through the computer. Based on the acquired stress–strain curves, the tensile forces in the steel bars were calculated, which is equal to the compressive forces exerted on the cement paste pipes. Then the stresses generated by the specimens were calculated.

The cross-sectional areas were different along the longitudinal direction of each steel bar, so the strain varied for different parts of a given steel bar when the longitudinal load was applied at the ends. Strain gauges were glued in the middle part of the steel bars, where the diameter was minimum. The local strain (strain gauge value) can be recorded continuously during the immersion tests, however, the total strain (entire steel bar strain) is needed for the calculation of specimen expansion. Therefore, the torque test calibration was carried out. The steel bars were assembled with an aluminum pipe whose length was 70 mm. Thereafter, a defined increment of certain torque value was applied at each step by means of a precision torque wrench. During this process, the local strain was recorded by computer. At the same time, the corresponding total strain was calculated based on the measurement of entire steel bar length change using a digital indicator. Then the linear relationship between the local strain and the total strain were calculated after the torque test calibration. During immersion tests, the local strain was recorded by computer, which was used for the calculation of the total strain. After that, the restrained expansion of specimen was calculated based on the obtained total strain.

2.3. MIP and EDS elemental mapping

The specimens without any restraint were taken out from the sulfate solutions at certain time and were prepared for MIP and microanalysis. Freeze-drying method was adopted for conditioning the specimens before the MIP test. MIP measurements were performed with a maximum intrusion pressure of 207 MPa. The contact angle and surface tension of mercury used for calculation were 139° and 480 mN/m, respectively [19,20]. For these pressures, the measured pore size was in the range from 0.007 μm to 400 μm.

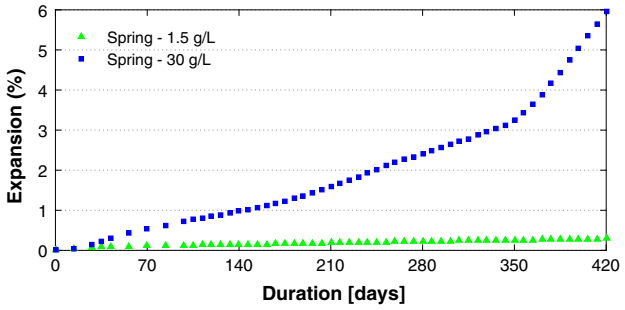

Fig. 3. Free expansions of the cement paste pipes in low and high sulfate solutions.

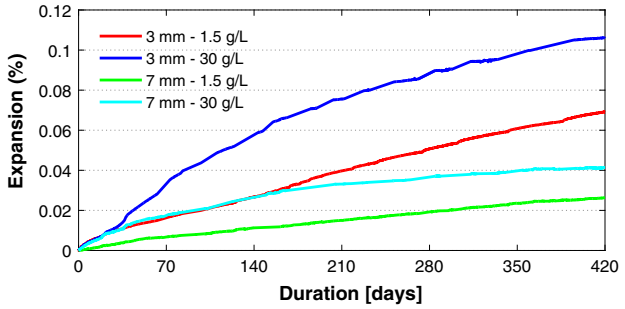

Fig. 4. Restrained expansions of the cement paste pipes in low and high sulfate solutions.

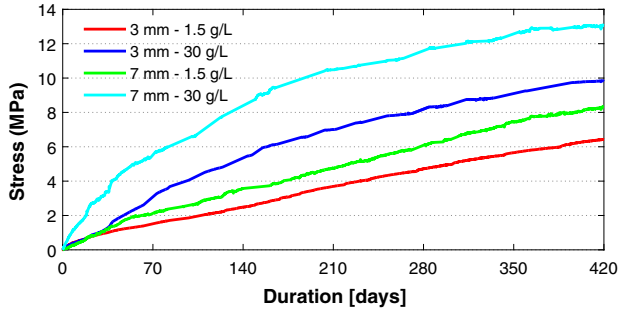

Fig. 5. Generated stresses of the restrained cement paste pipes in low and high sulfate solutions.

The sample preparations were needed before SEM-EDS microanalysis, which included cutting, drying, impregnating with low-viscosity epoxy resin, grinding, polishing and coating with carbon. Oven drying at 36 °C was used for the samples at 21-day, 70-day, 105-day and 133-day immersion. Solvent exchange with isopropanol and then drying under vacuum were used for samples at 189-day immersion and the reference sample just after 90-day curing. The prepared samples were then examined by SEM using backscattered electron (BSE) detector and EDS elemental mapping analyses. All SEM-EDS microanalyses were performed at an accelerating voltage of 15 kV and in the hi-vac chamber condition. The BSE micrographs and EDS elemental mappings were obtained at low magnification level (×100) which covers an area of 1264 × 948 μm^2 with the resolution of 256 × 192 pixels. Each pixel represents a single analysis spot. The X-ray element distribution maps were acquired by Thermo Scientific Noran 7 solid state EDS system in standardless analysis mode, which relies on the internal standards of the microanalysis software. The wall thickness of the specimens was 2.5 mm and both sides of the wall surface were exposed to sulfate solutions. Therefore, the length of 1264 μm along the diffusion direction was considered to be sufficient for the analysis, which is larger than the half wall thickness of specimens [17].

For the results of elemental mappings, the intensity of the sulfur mapping represents the relative relationship of weight percentage of sulfur. The sulfur mapping image from the EDS software output was a scaled 256 gray level image which could not show the weight percentage of sulfur directly. Therefore, a matlab code for image analysis was developed to get the normalized weight percentage of sulfur at each pixel and the sulfur distribution along the diffusion direction, which consists of two steps, rescaling and calculation. In rescaling step, based on the recorded highest normalized sulfur weight percentage of each mapping from the software which is related to the gray value of 255 in the scaled output mapping, the gray value in each pixel was rescaled linearly to a number which stands for the normalized weight percentage of sulfur. After this step, the normalized sulfur weight percentage at each pixel was obtained, as shown in Figs. 10 and 11. In calculation step, in order to get rid of the influence from the empty pores, only the pixels with sulfur weight percentage above 0 % were counted. Then the average of the counted pixels along each column (parallel to the exposed surface) was calculated, which means one number was obtained for each column. The obtained number represents the average sulfur weight percentage at the corresponding penetration depth. After this step, the sulfur distribution along the penetration depth was obtained based on the sulfur mapping image. For each sulfur distribution curve in this paper, the result is an average value obtained from two different areas of the same sample.

2.4. Micro-computed tomography technique

The internal structure of the cement paste pipes immersed in 30 g/L SO_4^{2-} after different immersion period was monitored by using a Micro CT-Scanner. Phoenix Nanotom X-ray system was used for data acquisition. During each scan, 1 440 tomographic images with an exposure time of 4 s were taken over a complete 360° rotation. Achieved voxel size was about 20 μm.

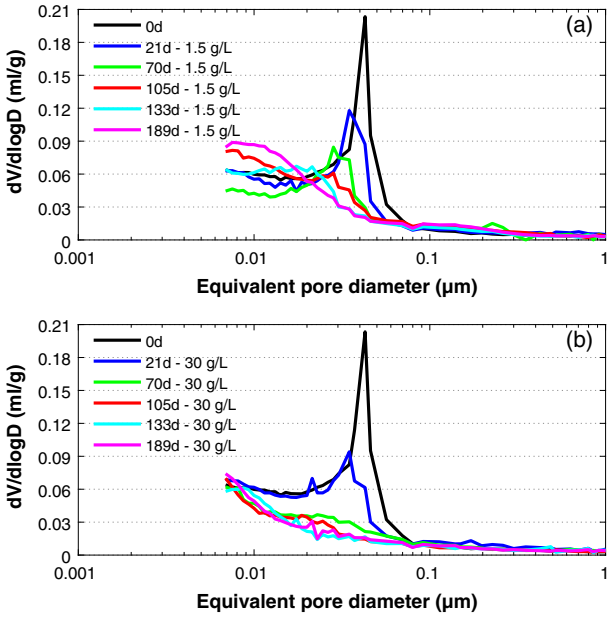

Fig. 6. Pore size distribution differential curves after being exposed to a) low and b) high sulfate solutions of unrestrained specimens.

After 189-day immersion, one sample was taken out from high sulfate solution, polished both ends and checked by CT scanning. After 294-day immersion, another sample from one whole cement paste pipe immersed in high sulfate solution was taken out and cut. The part with the height of around 39 mm was examined by CT scanning, which was also examined after 343-day and 420-day immersion.

The sample was taken out from the sulfate solution each time and immersed in a plastic bottle filled with deionized water, in order to make sure no drying damage happened to the specimen during the CT scanning. Then the specimen surrounding with deionized water was scanned. After each scan, the sample was put back to the sulfate solution immediately.

3. Results and discussion

3.1. Expansion and generated stress

It was observed that the expansions and the generated stresses in both low and high sulfate exposure conditions increased continuously during the immersion tests, as shown in Fig. 3, Fig. 4 and Fig. 5. Free expansions were expectedly found to be much larger than the restrained expansions. Free expansion in high sulfate solution (30 g/L SO_4^{2-}) was remarkably larger than free expansion in low sulfate solution (1.5 g/L SO_4^{2-}). In general, a higher sulfate solution or a lower restraint condition resulted in a faster expansion. A higher sulfate solution or a higher restraint condition lead to a larger generated stress. Fig. 5 shows the results of generated stresses up to 420-day immersion in the two different sulfate solutions under low- and high-restraint conditions. It was found that the generated stress almost stopped increasing for the specimens immersed in high sulfate solution under high-restraint condition after 364-day immersion and immersed in high sulfate solution under low-restraint condition after 403-day immersion. However, the tendency of the generated stress of specimens immersed in low sulfate solution is continuously increasing up to 420-day immersion. The generated stresses of specimens immersed in high sulfate solution and in low sulfate solution under high-restraint condition after 420-day immersion were 13.1 MPa and 8.3 MPa, respectively.

Several uniaxial tensile tests of the cement paste pipes just after 90-day curing in saturated limewater were also carried out. Tensile strength of around 5.7 MPa with the strain of around 0.031% was found. The free expansion of the specimen was 0.173% in low sulfate solution and 1.364% in high sulfate solution after 189-day immersion, which are far more than the elastic limit of the specimens under uniaxial tensile tests. However, no visually noticeable cracks were observed in both low and high sulfate solutions for free expansion specimens until 189-day immersion. Only for the sample immersed in high sulfate solution after 133-day immersion, continuous micro-cracks filled with mainly gypsum crystals began to be found by SEM, which can be seen in Fig. 9. The width of the layer was around 40 μm. This phenomenon can be understood as the dispersed local expansive stress lead to the local material to deform. The local expansive stress released after the deformation of local material. If a homogeneous material is completely free to deform, a uniform distribution of internal expansive stress may result in only deformation and no stress remains after the deformation. The heterogeneity of the material and the gradient of the local expansive stress distribution lead to the internal restraints in material, which results in redistribution of internal stresses and eigenstresses in the material. The eigenstress can exceed the material strength when the gradient of stress is large. Therefore, a small gradient of local expansive stress distribution may result in only deformation or distributed cracks. Localized cracks can happen when the stress gradient reaches the critical

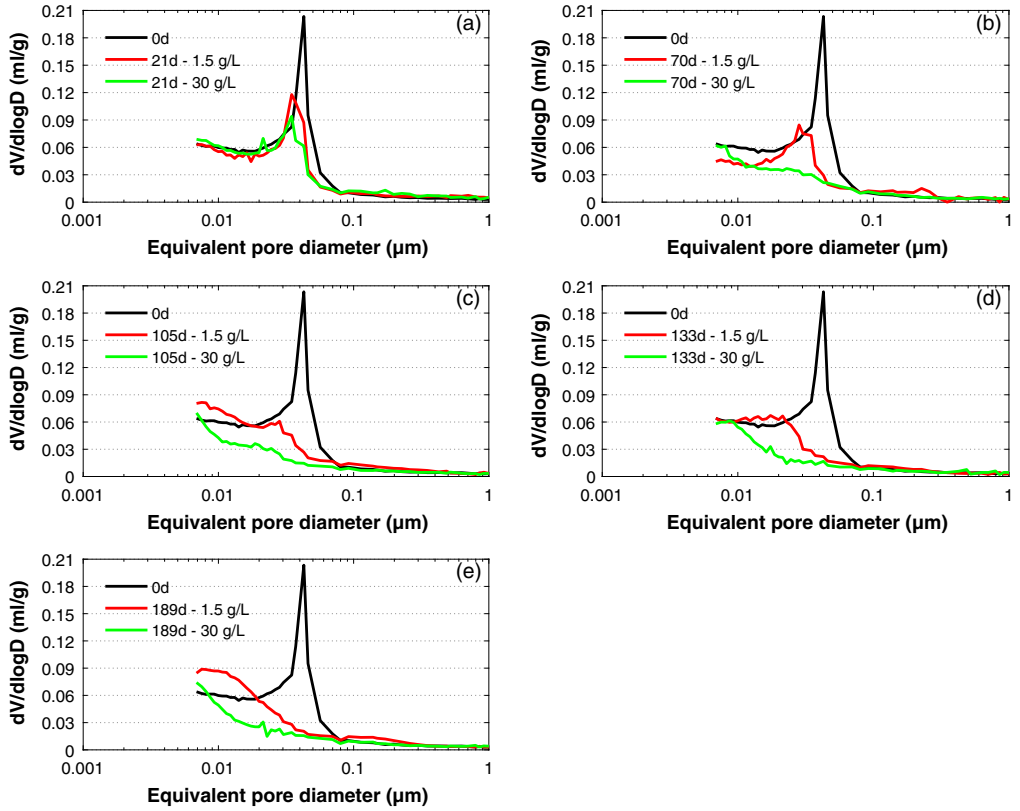

Fig. 7. Pore size distribution differential curves for a) 21-day, b) 70-day, c) 105-day, d) 133-day and e) 189-day immersion of unrestrained specimens.

level. The gradient of local expansive stress distribution was not large enough yet to cause the observed damage after 189-day immersion, which explained the phenomenon of a large free expansion without any visually noticeable cracks.

Under restrained conditions, the material cannot deform as much, which may cause the internal local expansive stress to build up, because of the restraint of crystal growth in nanopores. The specimens tended to expand, however, they were restrained by the steel bars. Therefore, the steel bars were under tension, while the specimens were under compression. The generated stresses were caused by the accumulation of internal local expansive stress, and acted as the compressive stresses on the specimens. After 189-day immersion, the generated stresses of 10.1 MPa in high sulfate solution and 4.4 MPa in low sulfate solution under high-restraint condition were measured. However, no visually noticeable cracks were observed for all the restrained specimens, which can be interpreted by the specimens under compression. 10.1 MPa was the generated stress from the restrained specimens, which was caused by the internal local expansive stress. If the internal local expansive stress worked the same for the free expansion specimens, the tensile stress in the free expansion specimens can be also as high as 10.1 MPa. Compared with the tensile strength of the specimens (around 5.7 MPa), the free expansion specimens should have been damaged remarkably at such stress levels. However, no visual damage was found for all the free expansion specimens until 189-day immersion, which indicated a different fracture mechanism for the free expansion condition.

Different fracture mechanisms under free and restrained expansion conditions can be proposed based on this research. For the free expansion condition, the specimen can deform freely, which leads to the relaxation of the internal local expansive stress. The heterogeneity of the material and the gradient distribution of the local expansive stress may cause the damage of the specimen in the final stage. While for the restrained expansion condition, the specimen is in fact under compression at the two ends. Meanwhile, the local expansive stress in the nanopores is possibly built up when the crystals are confined to grow and a higher supersaturation reaches. The whole specimen may be damaged under compression or tensile splitting in the final stage. That will be investigated further by modeling of the mechanisms.

3.2. Pore size distribution

The pore size distribution differential curve was derived from the pore size distribution cumulative intrusion curve and is essentially a plot of dV/dLogD (V: Pore volume) against D (D: Pore diameter). Fig. 6 shows the pore size distribution of the specimens before the exposure to sulfate solutions and after 21 days, 70 days, 105 days, 133 days and 189 days immersion. The peaks in the curves represent the pore diameters corresponding to the higher rate of mercury intrusion per change in pressure, which are also known as the "critical pore diameters" [21]. The area under the curve represents the total volume within the specific range of pores. In the low sulfate solution, it was found that the peak kept

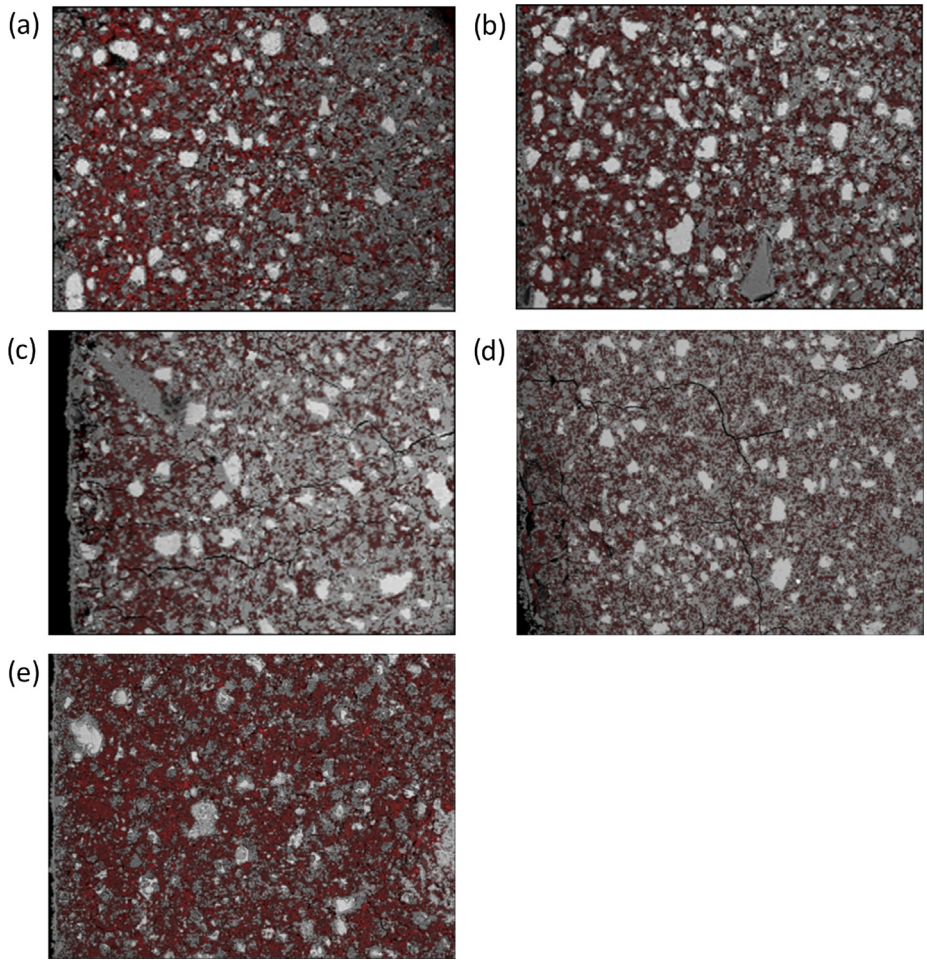

Fig. 8. Combined BSE and original sulfur mapping images for a) 21-day, b) 70-day, c) 105-day, d) 133-day and e) 189-day immersion in 1.5 g/L SO_4^{2-} of unrestrained specimens. Left edge of each image was the exposed surface. The field of view of each micrograph is 1264 × 948 μm^2.

moving to a smaller pore diameter as the duration of exposure increased. It is plausible to suggest that as the larger pores were continuously filled by the sulfate-bearing reaction products and meanwhile some smaller pores were produced because of the expansive stresses on the walls of larger pores in the range of 10 nm to 70 nm, as shown in Fig. 6. In the high sulfate solution, it was also found that the pores with diameters between 10 nm and 70 nm were continuously filled during the immersion tests. The difference was that the filling of the nanopores (10 nm – 70 nm) in the high sulfate solution was much faster than that in the low sulfate solution, which can be seen through Fig. 7. The filling of the nanopores can produce significant local expansive stress. High sulfate solution resulted in more filling of the nanopores compared with the low sulfate solution when the immersion time was same. This explained the observation of a faster expansion in high sulfate solution. The observation of the nanopores filling also supported the crystallization pressure theory to explain the origin of the expansive stress.

3.3. Sulfur distribution

The combined images of BSE micrographs and original sulfur mappings in weight percentage for the samples tested up to 189-day immersion are shown in Figs. 8 and 9, where the red color represents sulfur (one example is illustrated for each immersion time). The left side of the images represents the surface of the sample exposed to the sulfate solutions. Therefore the external sulfate ions diffused from left to right. The width of each image is a bit larger than the half wall thickness of specimens. The rescaled sulfur mappings in weight percentage are shown in Figs. 10 and 11, which are used for the calculations of sulfur distribution curves in Figs. 12 and 13.

It was observed from Figs. 8 and 9 that sulfur accumulated in the hydration products, which indicated the location of the newly formed sulfur-containing phases. It can be understood as that the external sulfate ions diffused into the pore network of the hydration products which is a mixture of several phases (eg: C-S-H, calcium hydroxide and monosulfate). When the supersaturation occurs, the ettringite or gypsum forms inside the pores or cracks. When the crystal formation is suppressed by the confined pore wall, the expansive stress on the pore wall is generated while the crystal is under compressive stress. The smaller the pore is, the higher the degree of supersaturation that is required for crystal formation. That means the larger the expansive stress is produced to maintain the equilibrium. Especially in nanopores, significantly larger expansive stresses may develop to damage the specimens.

Fig. 12a and b show the sulfur distribution from the unrestrained specimens after 0-day, 21-day, 70-day, 105-day, 133-day and 189-day immersion in low and high sulfate solution, respectively. The differences caused by different sulfate solutions at the same immersion days are presented in Fig. 13. The depth in the curve indicates the distance from the exposed surface. The sulfur in the curve stands for the average normalized weight percentage

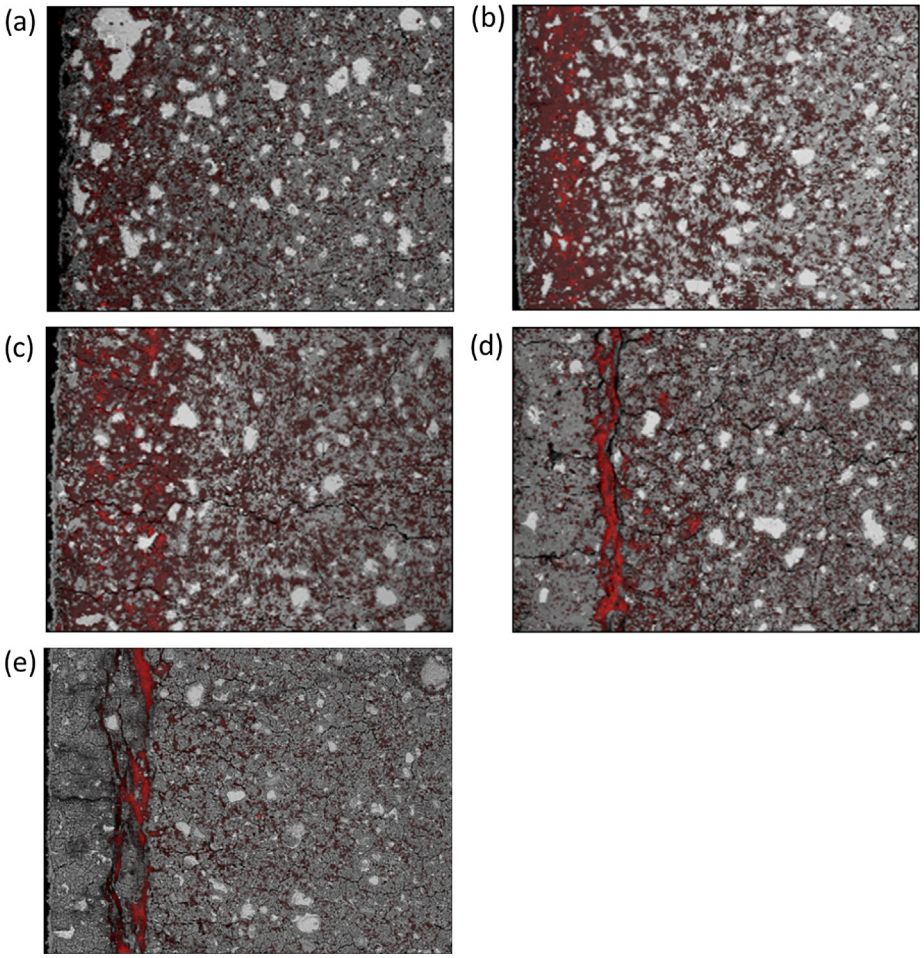

Fig. 9. Combined BSE and original sulfur mapping images for a) 21-day, b) 70-day, c) 105-day, d) 133-day and e) 189-day immersion in 30 g/L SO_4^{2-} of unrestrained specimens. Left edge of each image was the exposed surface. The field of view of each micrograph is 1264 × 948 μm^2.

of sulfur at a certain depth. The result of 0 day represents the specimen just after 90 days curing in saturated limewater.

As shown in Fig. 12a, in the low sulfate solution, the sulfur ingress profile had an obvious gradient along the penetration depth at 21-day immersion. Three zones can be seen from the surface to the inside of the samples, which were a leaching zone, an attack zone and a pristine zone. The pristine zone stands for the area unreached by the external sulfate ions, which disappeared before 70-day immersion. That can be understood as the external sulfate ions reached the half wall thickness of the sample within 70 days, considering that both sides of the wall surface were exposed to sulfate solutions. After 21-day immersion, the sulfur content of the area near the surface was increased slower compared with the area in the bulk part. With the immersion time increasing, the sulfur gradient along the penetration depth became smaller and smaller. The almost uniform sulfur distribution was found at 189-day immersion. A more uniform sulfur distribution with a higher average sulfur content was expected with extended immersion time. The sulfur content represents the amount of original and newly formed sulfur-containing phases at each location. In low sulfate solution, the main product was ettringite, which was limited by the abundance of aluminum-containing phases as well as available sulfate ion through external sulfate penetration. The amount of aluminum-containing phases was fixed at each location. Therefore, the sulfur content at each depth of the sample tended to increase to a limit value. Furthermore, the aluminum-containing phases were uniformly distributed inside the existing cementitious materials, which can lead to a uniform sulfur distribution in the final stage if no cracks happened.

During the immersion tests, there was always a dynamic sulfur gradient along the diffusion direction because of the penetration of external sulfate ions, which caused a local internal expansive stress gradient along the wall thickness of the specimens. Before the cracks occurred and gypsum precipitated in the formed cracks, it can be simply assumed that more sulfur relates to higher local expansive stress. In the initial stage, the attacked area tended to expand while the non-attacked area wanted to keep the original shape. Thus, the attacked area was restrained by the non-attacked area. In this situation, the attacked area was under compressive stress, and the non-attacked area was under tensile stress. The situation was similar for the sulfur-rich area and the area lower in sulfur. The sulfur-rich area expanded more than the area lower in sulfur and therefore was restrained by it. Therefore, for the zone at the boundary between sulfur-rich area and the area lower in sulfur, the tensile stress was probably very high, as a result of the gradient of the sulfur distribution. The micro-cracks started growing in the area where tensile stress exceeded tensile strength of the material, and in a later stage microcracks localized in main cracks.

For the specimens immersed in high sulfate solution, a layer of sulfur-rich phases was found after 133-day immersion, as shown in Fig. 9d. The layer was subparallel to the exposed surface with

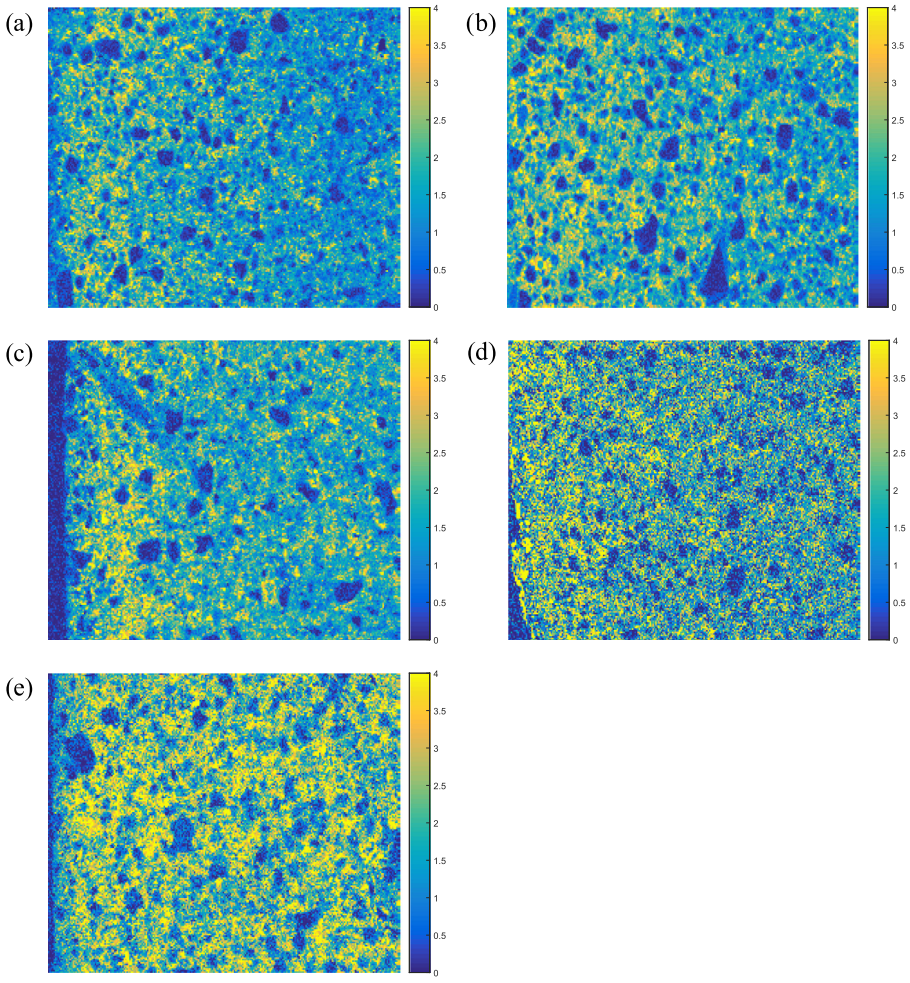

Fig. 10. Rescaled sulfur mapping images in weight percentage (wt. %) for a) 21-day, b) 70-day, c) 105-day, d) 133-day and e) 189-day immersion in 1.5 g/L SO_4^{2-} of unrestrained specimens. Left edge of each image was the exposed surface.

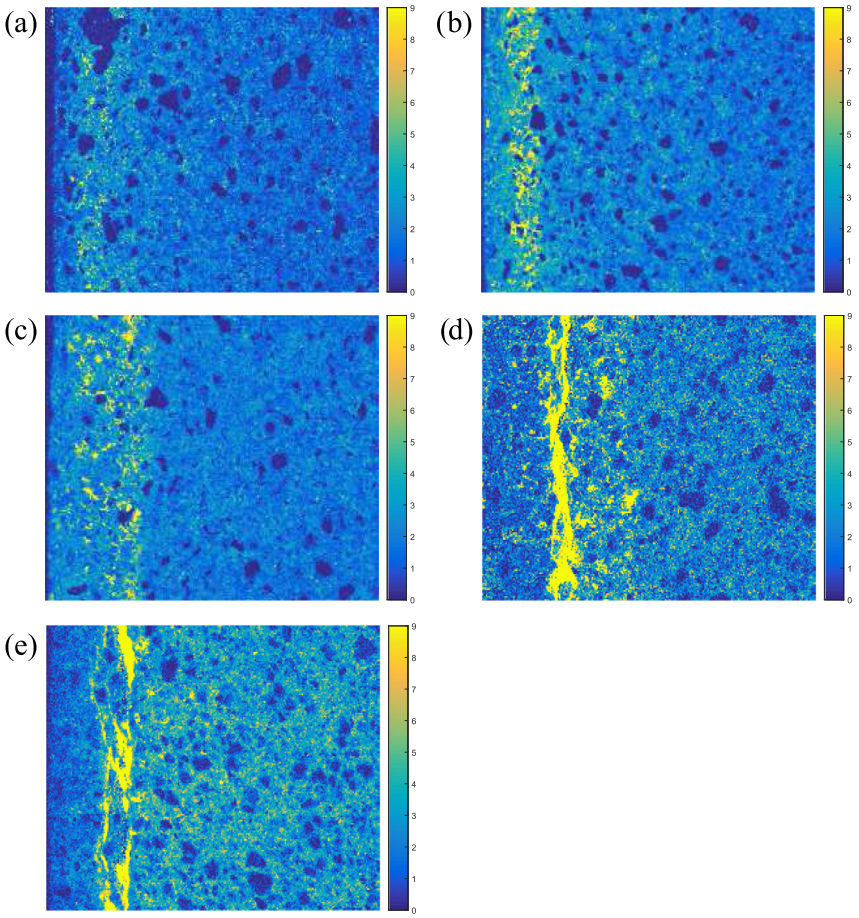

Fig. 11. Rescaled sulfur mapping images in weight percentage (wt. %) for a) 21-day, b) 70-day, c) 105-day, d) 133-day and e) 189-day immersion in 30 g/L SO_4^{2-} of unrestrained specimens. Left edge of each image was the exposed surface.

the distance from the exposed surface of around 250 μm. Calcium was also rich in the layer while the content of other elements were low, which suggested mainly gypsum precipitation. As shown in Fig. 12b, it was found that the sulfur content at a depth of between 30 μm and 250 μm kept increasing until 70-day immersion. The sulfur gradient was rather large at 70-day immersion, and a clear boundary was found at the depth of around 250 μm. The area with the higher sulfur content tended to expand more than the area with lower sulfur content, which caused tensile stress in the lower sulfur content area. The highest tensile stress may happen at the boundary between area under compressive stress and area under tensile stress. The large sulfur gradient at 70-day immersion may result in a very high stress gradient, which can probably make the micro-cracks form at the depth of around 250 μm. These micro-cracks were much larger compared with the pore network of the surrounding undamaged cement paste, therefore the crystal precipitation was promoted. After that, the distributed micro-cracks kept developing to form continuous micro-cracks because of the stress gradient. Finally, a localized crack occurred, as shown in Fig. 9d and e.

It can be found through Fig. 12b that the sulfur content at the depth of around 250 μm increased a lot at 105-day immersion and kept increasing, which can be understood from the fact that many distributed micro-cracks were formed at the depth of around 250 μm after 70-day immersion and gypsum kept precipitating in the formed micro-cracks. With the development of the cracks, more and more ions diffused into the cracks, which resulted in more and more gypsum precipitation. Finally, due to the produced crack pattern, a layer or several layers of gypsum can be found along the cracks. Moreover, the smaller sulfate-bearing crystals tended to dissolve and transfer their ions to a larger crystal in an adjacent pore [13,14,22], which explained the decrease of sulfur content at depth between 30 μm and 250 μm after 70-day immersion.

It can be concluded through Fig. 13 that high sulfate solution resulted in high sulfur content along the diffusion direction, when the immersion time was same as in the low sulfate solution. In the initial stage, the difference of sulfur distribution caused by the solution concentration is dominant by diffusion process and formation rates of sulfur-containing phases. It can be simply assumed that more sulfur relates to higher local expansive stress. Then the micro-cracks happened in the high sulfate solution, which was caused by the high local expansive stress and great stress gradient along the depth. After that, the gypsum began to precipitate in the localized micro-crack zone which lead to a rather high sulfur content appearing at certain depth in the high sulfate solution. This process indicates that the specimens under external sulfate attack is damaged layer by layer. The sulfur distribution curves in this paper are important for our simulation work which is also in progress. A gradient of local expansive stresses along the depth has to be assumed based on the sulfur distribution at different immersion time, which is an important simulation input. The measured sulfur distributions were from the unrestrained specimens. For the specimens under restrained conditions, the diffusion speed will most probably be slower compared with the free condition before the development of the connected micro-cracks.

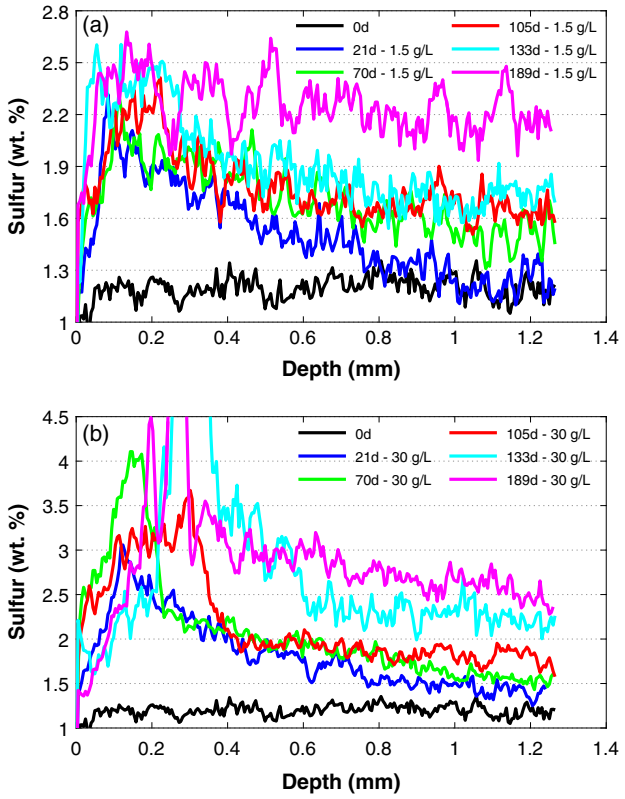

Fig. 12. Sulfur distributions along diffusion direction after being exposed to a) low and b) high sulfate solutions of unrestrained specimens.

3.4. Crack pattern

Two layers of mainly gypsum crystals were observed under SEM in the specimen immersed in high sulfate solution after 189-day immersion (Fig. 9e). In order to get a non-destructive view of the crack pattern caused by external sulfate attack, one sample after 189-day immersion in high sulfate solution was checked by CT scanning. However, cracks were not detected and only grey value differences across the wall of the sample were found, which was most likely due to the limited resolution achieved by the CT scanning compared to SEM.

After 294-day immersion, one whole cement paste pipe immersed in high sulfate solution was taken out and cut. The part with the height of around 39 mm was examined by CT scanning and damage was observed at the top part of the sample (Fig. 14a). Then the same sample was checked after 343-day (Fig. 14b) and 420-day (Fig. 14c) immersion. The three dimensional renderings with two views in each situation are shown in Fig. 14. It can be found from Fig. 3 that the free expansion in high sulfate solution began to increase fast from 189-day immersion and increased much faster from 350-day immersion. Combined with Figs. 9 and 14, it seems that the attack process in high sulfate solution under free expansion condition can be divided into three stages. In the first stage, both large pores and small pores continued to be filled, which lead to a reduced porosity and a continuous increase of the amount of small pores under significant expansive stress. Distributed micro-cracks or few localized cracks may happen. The free expansion increased relatively steadily. In the second stage, more and more micro-cracks and localized cracks were formed, which can be seen in Figs. 9e and 14a. Therefore, the free expansion began to increase fast. In the third stage, the localized

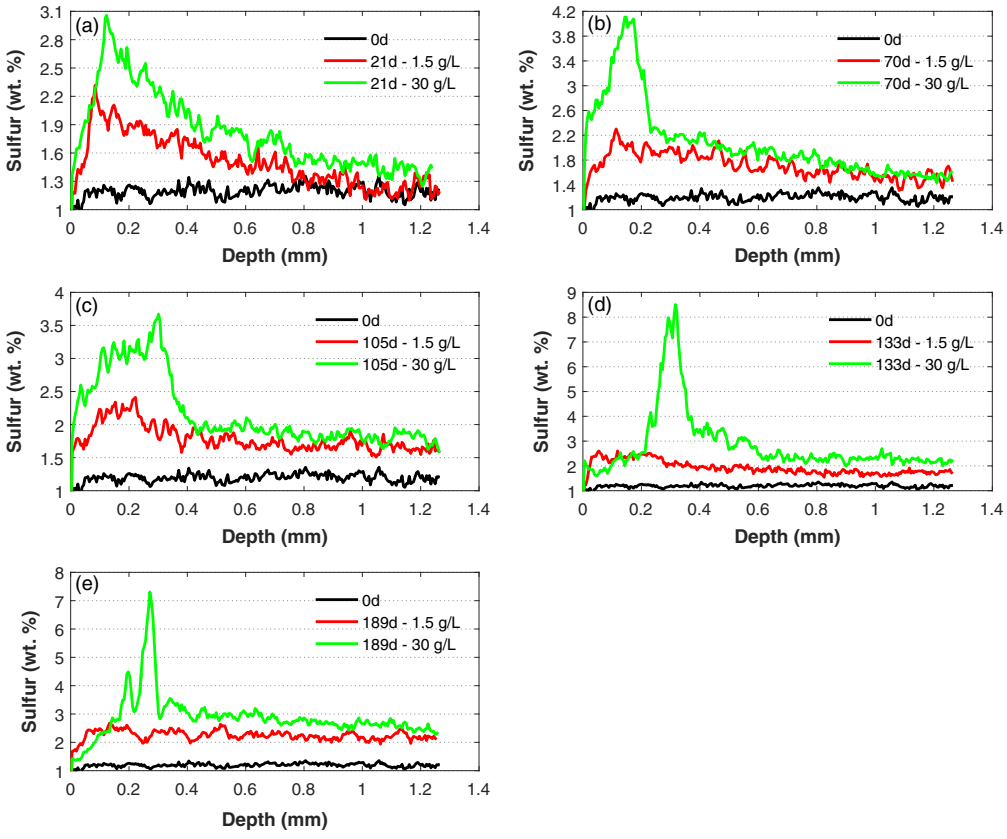

Fig. 13. Sulfur distributions along diffusion direction for a) 21-day, b) 70-day, c) 105-day, d) 133-day and e) 189-day immersion of unrestrained specimens.

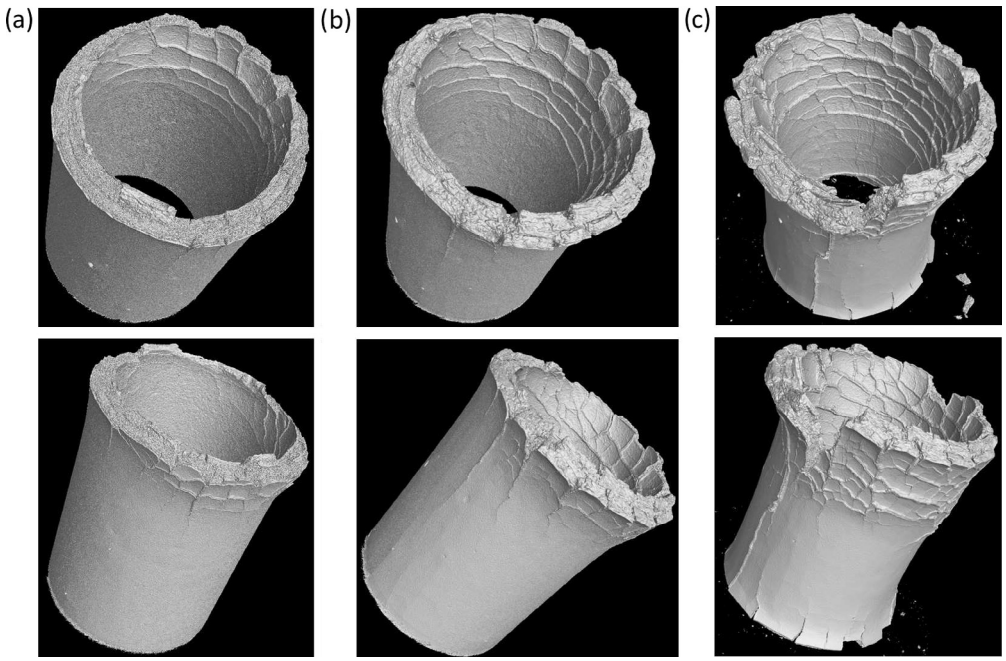

Fig. 14. 3D renderings of unrestrained cement paste pipe by CT scanning after a) 294-day, b) 343-day and c) 420-day immersion in 30 g/L SO_4^{2-}.

cracks began to connect with each other, which lead to the increasing formation of large cracks. The free expansion increased much faster and the big damage began to appear, which can be seen in Fig. 14b and c. For the specimens immersed in low sulfate solution, the free expansion was still rather small and no visual cracks were found until 420-day immersion, which were maybe still in the first stage.

For the specimen after 294-day immersion in high sulfate solution, five reconstructed microtomography slices were chosen randomly from top to bottom of the specimen along the longitudinal direction, which were illustrated in Fig. 15a also from top to bottom. After that, for the 343-day immersion and 420-day immersion, the microtomography slices with similar location as 294-day immersion were chosen and shown in Fig. 15b and c, respectively. The crack propagation can be seen along the horizontal direction in Fig. 15. It showed a similar tendency from Fig. 15 compared with Fig. 9. Several localized cracks which were subparallel to the exposed surface were found. The vertical cracks starting from the exposed surface were also found. Therefore, the crack pattern should be a combination of the horizontal cracks which started some distance away from the exposed surface and the vertical cracks which started from the exposed surface.

4. Conclusions

The expansions and generated stresses in all the conditions kept increasing during the exposure of the specimens to external sulfate solutions. In general, a higher sulfate solution or a lower restraint condition resulted in an earlier expansion. A larger generated stress can be found in a higher sulfate solution or a higher restraint condition. According to the MIP measurements, the pores with diameters between 10 nm and 70 nm were continuously filled during the immersion tests, and high sulfate solution lead to a faster filling. The sulfur content inside the specimens kept increasing during the immersion tests in both low and high sulfate solutions. High sulfate solution resulted in high sulfur content along the diffusion direction under same duration of immersion. In low sulfate solution, an almost uniform sulfur distribution along depth was found at 189-day immersion. However, in high sulfate solution, a layer or several layers of mainly gypsum precipitation can be found from 133-day immersion.

For the specimens under unrestrained condition, the specimens can deform freely. The local expansive stress was relaxed after the deformation of the local material. The heterogeneity of the material and the gradient of the local expansive stress distribution may lead to the formation of cracks. During the immersion tests, there was always a dynamic sulfur gradient along the diffusion direction, which caused a dynamic gradient of local expansive stress distribution. In high sulfate solution, a large sulfur gradient was found at 70-day immersion, which probably made the distributed micro-cracks form at the zone with the distance from the exposed surface of around 250 μm. The distributed micro-cracks developed to be the continuous micro-cracks and then large cracks at later stage. The gypsum kept precipitating in the micro-cracks during this process. A layer of mainly gypsum was formed subparallel to the exposed surface at 133-day immersion. Visual damage began to appear after 294-day immersion. However, in low sulfate solution, no visual cracks were found even after 420-day immersion.

For the specimens under restrained condition, the specimens were in fact under compressive stress at the two ends and cannot deform that much, which possibly made the local expansive stress in the nanopores built up. The whole cement paste pipe may be damaged under compression or tensile splitting in the final stage. The generated stresses of the specimens at the restrained boundaries were 13.1 MPa and 8.3 MPa in high and low sulfate solution under high-restraint condition at 420-day immersion.

The sulfur distribution, pore size distribution, free expansion, restrained expansion and generated stress at 21-day, 70-day, 105-day, 133-day and 189-day immersion were obtained through experiments in this research, which have a significant meaning for the further study, especially for the assistance of numerical simulations.

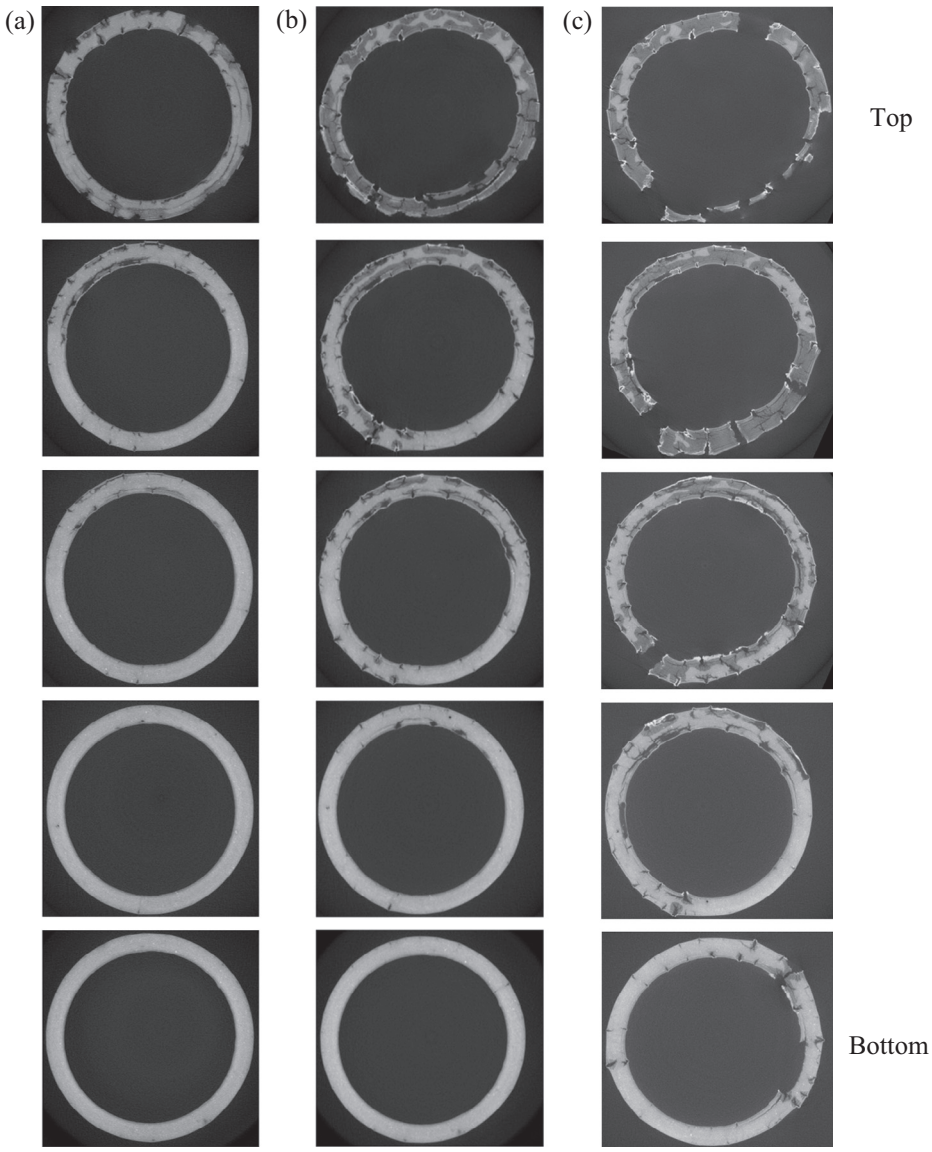

Fig. 15. Reconstructed microtomography slices from top to bottom of unrestrained cement paste pipe after a) 294-day, b) 343-day and c) 420-day immersion in 30 g/L SO_4^{2-}.

Acknowledgements

The National Basic Research Program (973 Program) of China via Grant No. 2011CB013604 and the scholarship from the Oversea Study Program of Guangzhou Elite Project are greatly acknowledged.

References

[1] J. Skalny, J. Marchand, I. Odler, Sulfate Attack on Concrete, 1st ed., Spon Press, London, 2002.
[2] E. Rozière, A. Loukili, R. El Hachem, F. Grondin, Durability of concrete exposed to leaching and external sulphate attacks, Cem. Concr. Res. 39 (12) (2009) 1188–1198.
[3] H. Binici, O. Aksoğan, Sulfate resistance of plain and blended cement, Cem. Concr. Compos. 28 (1) (2006) 39–46.
[4] T. Schmidt, B. Lothenbach, M. Romer, J. Neuenschwander, K. Scrivener, Physical and microstructural aspects of sulfate attack on ordinary and limestone blended portland cements, Cem. Concr. Res. 39 (12) (2009) 1111–1121.
[5] M. Santhanam, M.D. Cohen, J. Olek, Sulfate attack research – whither now?, Cem Concr. Res. 31 (6) (2001) 845–851.
[6] A. Neville, The confused world of sulfate attack on concrete, Cem. Concr. Res. 34 (8) (2004) 1275–1296.
[7] E. Irassar, V. Bonavetti, M. Gonzalez, Microstructural study of sulfate attack on ordinary and limestone portland cements at ambient temperature, Cem. Concr. Res. 33 (1) (2003) 31–41.
[8] W. Müllauer, R.E. Beddoe, D. Heinz, Sulfate attack expansion mechanisms, Cem. Concr. Res. 52 (2013) 208–215.
[9] C. Yu, W. Sun, K. Scrivener, Mechanism of expansion of mortars immersed in sodium sulfate solutions, Cem. Concr. Res. 43 (2013) 105–111.
[10] B. Lothenbach, B. Bary, P. Le Bescop, T. Schmidt, N. Leterrier, Sulfate ingress in portland cement, Cem. Concr. Res. 40 (8) (2010) 1211–1225.
[11] A. Chabrelie, Mechanisms of Degradation of Concrete by External Sulfate Ions Under Laboratory and Field Conditions (Ph.D. thesis), Ecole Polytechnique Federale De Lausanne, Lausanne, Switzerland, 2010.
[12] G.W. Scherer, Crystallization in pores, Cem. Concr. Res. 29 (8) (1999) 1347–1358.
[13] G.W. Scherer, Stress from crystallization of salt, Cem. Concr. Res. 34 (9) (2004) 1613–1624.
[14] R.J. Flatt, G.W. Scherer, Thermodynamics of crystallization stresses in DEF, Cem. Concr. Res. 38 (3) (2008) 325–336.
[15] M. Steiger, Crystal growth in porous materials-II: influence of crystal size on the crystallization pressure, J. Cryst. Growth 282 (3) (2005) 470–481.
[16] Y. Maltais, E. Samson, J. Marchand, Predicting the durability of portland cement systems in aggressive environments – laboratory validation, Cem. Concr. Res. 34 (9) (2004) 1579–1589.
[17] X. Ma, O. Çopuroğlu, E. Schlangen, N. Han, F. Xing, Experimental and numerical study on cement paste degradation under external sulfate attack, in: Proceedings of 9th International Conference on Fracture Mechanics of Concrete and Concrete Structures, 2016.

[18] R.E. Beddoe, R. Lippok, Hygral stress in hardened cement paste, Mater. Struct. 32 (9) (1999) 627–634.
[19] G. Ye, Experimental Study and Numerical Simulation of the Development of the Microstructure and Permeability of Cementitious Materials (Ph.D. thesis), Delft University of Technology, The Netherlands, 2003.
[20] Z. Yu, Microstructure development and transport properties of portland cement – fly ash binary systems – in view of service life predictions (Ph.D. thesis), Delft University of Technology, The Netherlands, 2015.
[21] R.A. Cook, K.C. Hover, Mercury porosimetry of hardened cement pastes, Cem. Concr. Res. 29 (6) (1999) 933–943.
[22] G.W. Scherer, Factors affecting crystallization pressure, in: International RILEM TC 186-ISA Workshop on Internal Sulfate Attack and Delayed Ettringite Formation, Villars, Switzerland, (2002) 139–154.